Available online at www.sciencedirect.com
ScienceDirect
Journal of the European Ceramic Society 31 (2011) 1033–1039
www.elsevier.com/locate/jeurceramsoc

Original Article

Shock-consolidated TiO_2 bulk with pure anatase phases fabricated by explosive compaction using underwater shockwave

Youngkook Kim [a,*], Fumiaki Mitsugi [b], Ikegami Tomoaki [b], Kazuyuki Hokamoto [a], Shigeru Itoh [a]

[a] *Shock Wave and Condensed Matter Research Center, Kumamoto University, Kurokami 2-39-1, Kumamoto City 860-8555, Japan*
[b] *Graduate School of Science & Technology, Kumamoto University, Kurokami 2-39-1, Kumamoto City 860-8555, Japan*

Received 21 April 2010; received in revised form 9 December 2010; accepted 17 December 2010
Available online 15 January 2011

Abstract

Titanium dioxide (TiO_2) bulk with pure anatase phases was fabricated by an explosive compaction technique using an underwater shockwave. Dynamic shock pressure of 6 GPa was used to consolidate anatase TiO_2 powders. Its microstructural, crystalline structural and photocatalytic characteristics were observed and measured by various techniques, such as X-ray diffraction (XRD), scanning electron microscopy (SEM) and photocatalytic activity measurement system. It was confirmed that the relative density of anatase TiO_2 compact is about 96% (3.73 g/cm^3) of the theoretical density (3.89 g/cm^3) and a strong surface bonding between particles is formed by a shock energy. In X-ray diffraction analysis, high purity anatase phases, broadened peaks due to lattice defects and decreased crystallite size were found. For the photocatalytic activities, the anatase TiO_2 compact was quite excellent compared to the commercial sintered TiO_2 bulk.

Keywords: Grain growth; Defects; TiO_2; Residual stress

1. Introduction

Titanium dioxide (TiO_2) and related materials have attracted considerable attention because of their specific commercial applications, such as environmental photocatalysis,[1] solar cells[2] and gas sensors.[3] It is well-known that TiO_2 is present in nature with three crystalline structures; rutile, anatase and brookite. In particular, in terms of photocatalytic activity, the anatase structure, which exhibits thermodynamically metastable and transform irreversibly to rutile upon heating, is more active than the rutile structure.[4] However, it is very difficult to sinter anatase-structured TiO_2 bulk with high purity anatase phases because phase transformation from anatase to rutile occurs easily in a low temperature regime (500–600 °C), which depends on the preparation conditions such as particle size, impurities, and atmospheric conditions.[5] Several other sintering methods exist for nano-structured TiO_2 ceramics, such as conventional hot sintering (CHS),[6,7] spark plasma sintering (SPS),[8–10] two-step sintering (TSS)[11] and high pressure-low temperature sintering.[12] These are geared towards densification and suppression of grain growth of TiO_2. Most of these sintered samples exhibited both anatase and rutile phases, and only the rutile phase. Thus, despite the excellent optical properties of anatase, very few studies have examined.

Explosive compaction technique is also one of the fabrication methods for ceramics. Since the explosive compaction for iron oxide–aluminum powder mixtures using an explosive press was attempted,[13] it has been primarily investigated to obtain difficult-to-consolidate ceramics [14–16] and for diamond synthesis.[17] In this technique, one of the unique characteristics is that grain growth is not generated in the compacts due to the very fast consolidation process within microsecond time scale,[18,19] and also it is possible to obtain denser materials while avoiding prolonged heating and to retain the structural characteristics of the starting powders.[19,20] In particular, the explosive compaction technique using an underwater shockwave has been reported to be more useful for consolidation of hard ceramic powders due to several advantages, including control of shock pressure and homogenous transfer of a shockwave.[21] However, there exists a serious problem in explosive compaction. That is cracking of the compacts. It is usually generated by tensile stresses and thermal residual stresses due to rapid cooling process after shock-loading. In order to overcome the problem, Hokamoto and

* Corresponding author.
E-mail addresses: kim@shock.smrc.kumamoto-u.ac.jp, deto.wave@gmail.com (Y. Kim).

0955-2219/$ – see front matter © 2010 Elsevier Ltd. All rights reserved.
doi:10.1016/j.jeurceramsoc.2010.12.020

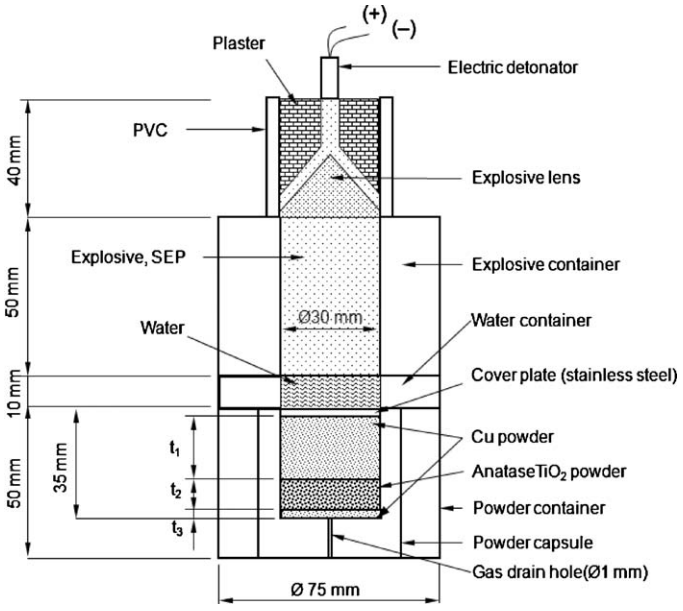

Fig. 1. Schematic illustration of underwater shock compaction device.

co-workers,[22–24] have employed a high temperature shock consolidation. This method preheats the ceramic powders before compaction. The high temperature can lead to a decrease in hardness and strength of ceramic powders and an increase in deformability and enhancement of surface melting. Indeed, this method has shown considerable improvement. In the present work, we have introduced another method in order to minimize the cracking problem. That is the use of residual heat of copper (Cu) powders generated during and after compaction. The Cu powders in the form of top and bottom layers of the ceramic powder yield residual heat with a high temperature within a very short time when a shockwave passes through the powders, because of its lower heat capacity. The high temperature residual heat induces thermal effects leading to retardation of rapid cooling process, minimization of residual stresses and assistance of interparticle melting or surface bonding between particles. This method is more simple and effective than high temperature shock consolidation. In our recent investigation, this method has shown a good consolidation quality without visible cracks. Thus, the aim of this work is to obtain an anatase TiO_2 bulk with high purity phases without cracks using high temperature residual heat and investigate its structural and photocatalytic characteristics.

2. Experimental procedure

2.1. Underwater shock compaction device

Fig. 1 shows a schematic illustration of explosive compaction device using an underwater shockwave. The device typically consists of several parts including an electrical detonator, explosive lens, explosive container, water container, powder container and powder capsule. A high performance explosive, SEP (detonation velocity: 6.97 km/s, density: 1300 kg/m^3; Asahi-Kasei Chemicals Corp., Japan) was used and charged in the explosive container. The explosive lens was used to generate a planar shockwave using two types of explosives, SEP and HABW (detonation velocity: 4.75 km/s and density: 2200 kg/m^3; Asahi-Kasei Chemicals Corp., Japan), with different detonation velocities. The water container was filled with water to create an underwater shockwave, with a size of 10 mm height and 30 mm inner diameter. Each powder, anatase TiO_2 (200 nm size, Ishihara Sangyo Kaisha Ltd., Japan) and copper (Cu) (45 μm size, Wako Chemical Co. Ltd., Japan), was filled and pressed in the powder capsule one by one using a uniaxial press machine at 50 MPa. The green density of each compressed powder was about 50% of the theoretical density for each material determined by the compressed volume and height of each layer t_1, t_2, and t_3 in the powder capsule. The powder capsule has an inner diameter of 30 mm, height of 50 mm, powder charging depth of 35 mm, and a gas drain hole (1 mm) to allow air to be exhausted during shock-loading. A steel cover plate (1 mm thickness) was placed on the Cu powder to prevent the penetration of impurities such as water and product gases of explosive.

2.2. Shock pressure measurement

A peak shock pressure of underwater shockwave was evaluated by a shock pressure measurement system using a piezofilm stress gauge (PVF2-11-,125-EK, Dyansen Inc., USA). Fig. 2 shows a schematic illustration of shock pressure measurement system. The piezofilm stress gauge was set below the cover plate. When the ignition is started by an electric detonator, initial and final peak values are detected by enamel wire and piezofilm stress gauge, respectively and measured by an oscilloscope measurement device.

2.3. Structural characterization

Microstructures of each sample were observed by scanning electron microscopy (SEM, JCM-5700, JEOL, Japan). The relative density and X-ray diffraction analysis of shock-consolidated anatase TiO_2 were evaluated by Archimedes method and X-ray diffractometer (RIGAKU Rint 2100) with Cu Kα radiation and scanning step size of 0.02°, respectively. The crystallite size and micro-strain of the shock-consolidated anatase TiO_2 were estimated by means of the Williams–Hall (W–H) plot method. In X-ray diffraction analysis, the effect of instrumental broadening was investigated using a standard silicon reference material (NIST 640d, USA) and subtracted from the peak broadening contributions.

2.4. Photocatalytic activities

The photocatalytic activities of the shock-consolidated anatase TiO_2 and were evaluated and compared to the commercial sintered TiO_2 using a photocatalytic activity evaluation system. This system consists of a high-resolution spectrometer (HR-4000, Ocean Optics, USA), reflection fiber probe (R400-7-UV/Vis, Ocean Optics, USA), light source for the measurements (DT-Mini, Ocean Optics, USA) and UV LED (375-01S, 375 nm, 22 mW/cm^2, ø8 mm, South Walker). The UV-LED was focused

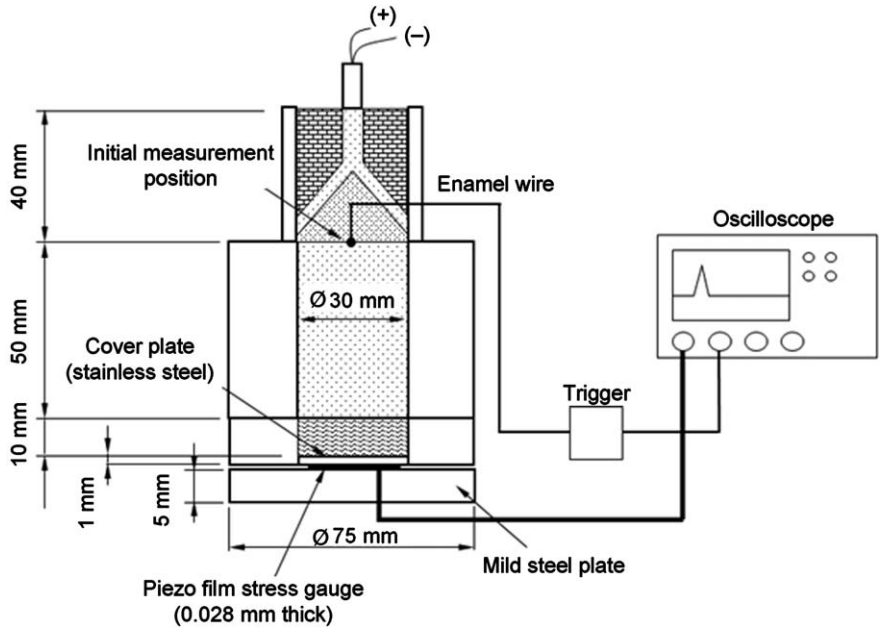

Fig. 2. Schematic illustration of shock pressure measurement system.

on the surface of a sample (5 mm × 5 mm × 5 mm size) to decompose methylene blue solution (0.1 mmol/L, 1 μL) that was dropped on the surface of the sample. The decomposition of the methylene blue was tested by light reflection obtained from the sample.

3. Results and discussion

3.1. Explosive compaction

Fig. 3 shows a profile of peak shock pressure of underwater shockwave. The measured shock pressure value raised up to maximum peak within 0.5–1 μs was about 6 GPa. One of the important things in explosive compaction is to make the homogeneous distribution of a planar shockwave for impacting areas. Otherwise, a poor consolidation quality will be certainly obtained. The planar shockwave can be obtained by the configuration change of water container.

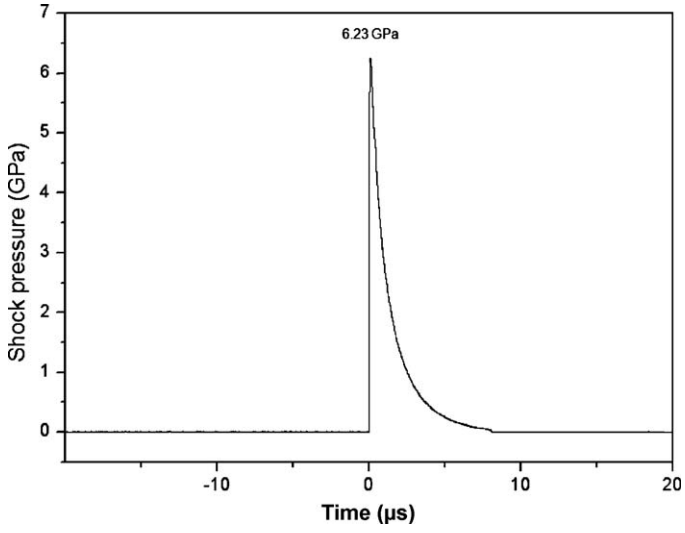

Fig. 3. Profile of peak shock pressure of underwater shockwave measured by piezofilm stress gauge.

Fig. 4 shows photographs of shock-consolidated anatase TiO_2 and Cu compact with thickness of t_1. The anatase TiO_2 compact was processed with a square shape with a size of 15 mm × 15 mm × 5 mm thickness as shown in Fig. 4(a). The relative density was 96% (3.73 g/cm^3) of the theoretical density (3.89 g/cm^3) and low hardness value of 100–120 H_v at 0.49 N was confirmed. It was also confirmed that crack-free formation is formed at most of the areas in the anatase TiO_2 compact, whereas a spalling generated by tensile stresses was observed in the Cu compact shown in Fig. 4(b). As above mentioned, tensile stresses are a factor leading to macro-cracks in the compacts and usually generated by the interaction of two release waves induced by high velocity impact of a flyer plate and target.[25] Accordingly, the generation sites of spalling is related to the thickness of a flyer plate because one of the release waves is generated by a reflected wave coming from the flyer plate. In this compaction system, the tensile stresses can be generated when the cover plate with thickness of 1 mm accelerated by underwater shockwave impacts on the powders. However, there was no influence of spalling in the anatase TiO_2 compact. Indeed, the generated position of spalling was almost equal to the thickness of cover plate. This result gives a good evidence to understand the generation of spalling in the compacts and we believe that the generation of spalling can be reduced by well-designed compaction system.[26]

3.2. Structural characteristics

Fig. 5 shows scanning electron micrographs of Cu starting powder and Cu compacts, respectively. It was observed that the Cu powders has a flake shape as shown in Fig. 5(a)

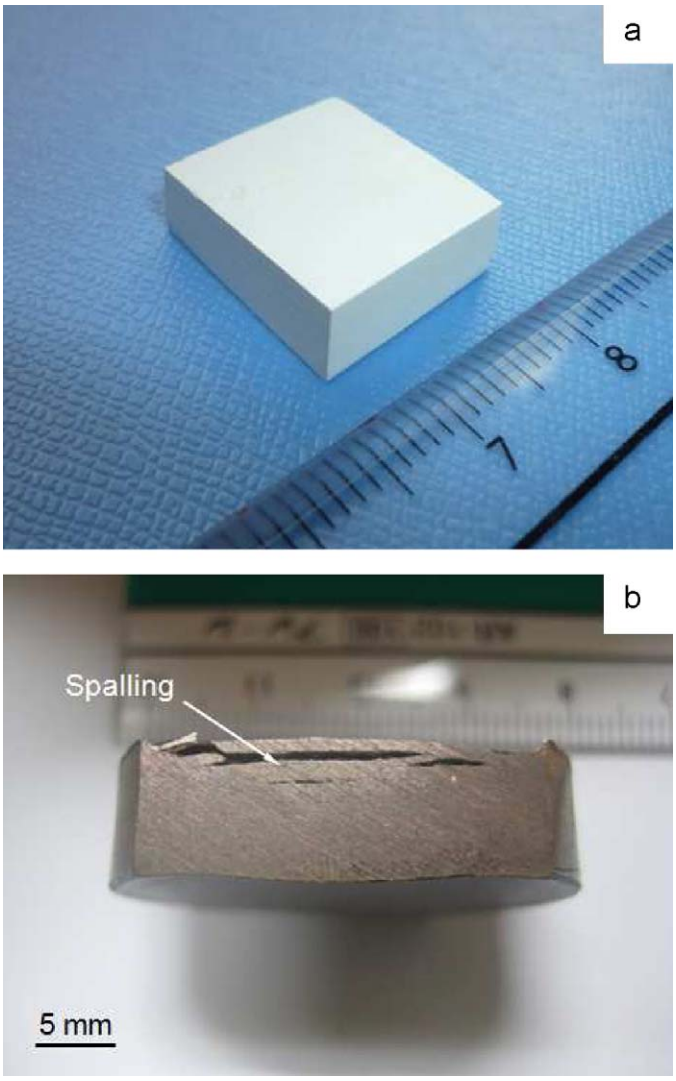

Fig. 4. Photographs of shock-consolidated materials; (a) shock-consolidated anatase TiO_2 and (b) Cu compact with thickness of t_1.

and completely melted, and voids and pores are generated in the Cu compacts. This is shown in Fig. 5(b) and (c), respectively. These results enable the prediction for the generation of a high temperature, which can lead to thermal effects of Cu compacts. Fig. 6 shows microstructures of shock-consolidated anatase TiO_2 and its starting powder. As shown in Fig. 6(a), no voids formation was observed in the compact, since the powders were substantially deformed to fill any voids, and it was clearly observed that a surface bonding between powder particles was formed and particle sizes were not changed in comparison with those of starting powder. Although agglomerated particles exist in the starting powder as shown in Fig. 6(b), there were no more agglomerated particles in the compact due to a shock energy, microkinetic energy and frictional energy generated within particles or particles surfaces. These results indicate that the explosive compaction using an underwater shockwave can lead to localized deformation and strong surface bonding only at the particle surfaces, since the color of the compact is still white. In X-ray diffraction analysis, which is shown in Fig. 7,

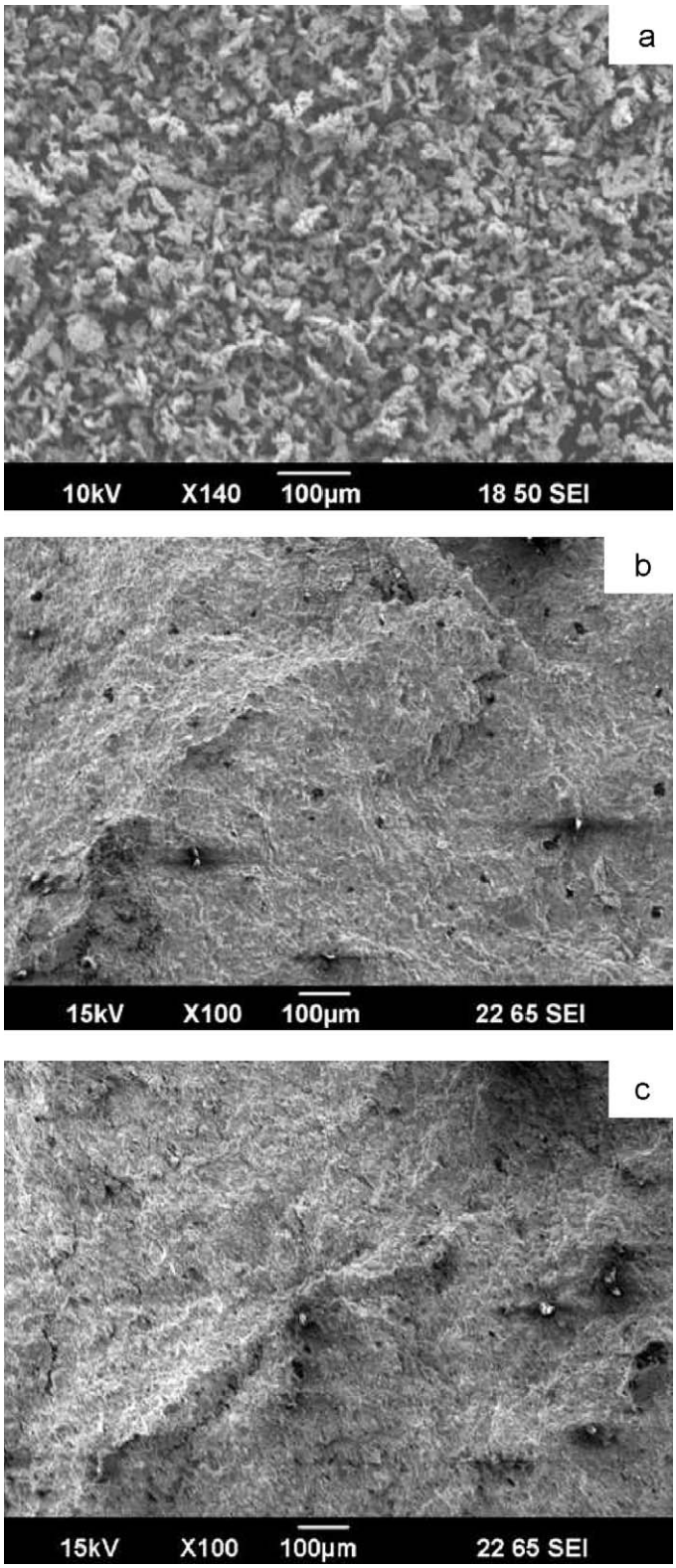

Fig. 5. Scanning electron micrographs (SEMs) of (a) Cu starting powder and Cu compacts with thickness of (b) t_1 and (c) t_3, respectively.

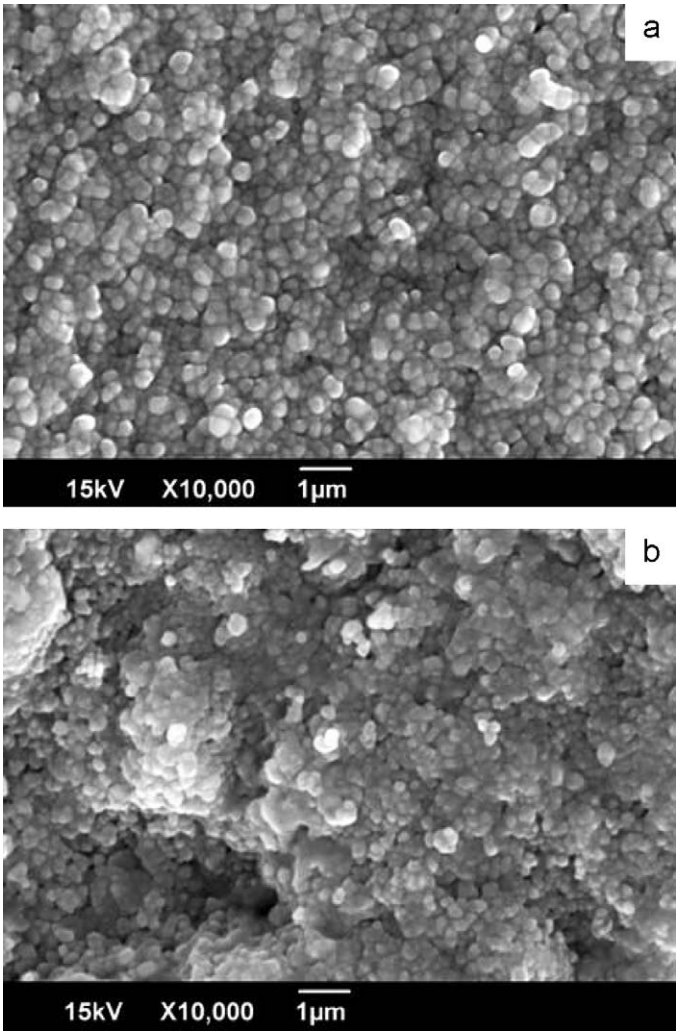

Fig. 6. Scanning electron micrographs (SEMs) of the fracture surfaces; (a) is the shock-consolidated anatase TiO_2 and (b) is the anatase TiO_2 starting powder.

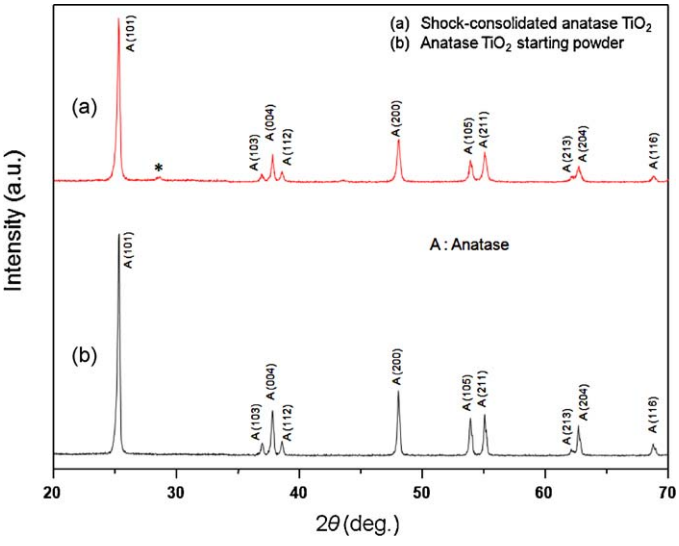

Fig. 7. X-ray diffraction patterns; (a) is shock-consolidated anatase TiO_2 and (b) is anatase TiO_2 starting powder.

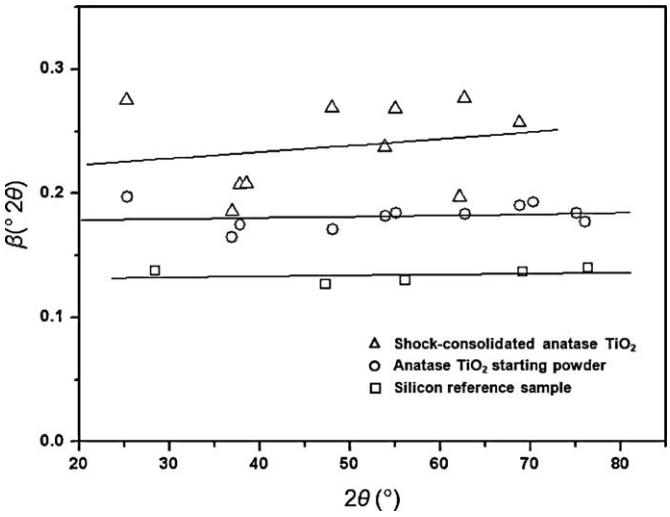

Fig. 8. Integral breadths of the shock-consolidated anatase TiO_2, anatase TiO_2 starting powder and silicon reference sample (NIST 640d) as functions of 2θ.

we have confirmed that high purity anatase phases are detected and there was no a phase transformation, and the peak patterns correspond to those of starting powder. However, a very weak diffraction peak (*) at 28.62° was observed. This peak does not correspond to any rutile peak. The peak is likely a transient phase of TiO_2, because such a transient phase can easily be formed by high pressure at the surfaces between anatase particles during collision. [27] The diffraction peaks of the anatase TiO_2 compact were slightly broadened. These broadened peaks are attributed to lattice defects such as distortions and dislocations, or decreased crystallite size due to a shock energy, which induces a rapid and intense deformation at particle surfaces, and such broadened peaks are easily detected in the shock-consolidated ceramics and metals.[19,28] Generally, the peak broadening in X-ray diffraction analysis can be attributed to several factors such as instrumental broadening, finite crystallite size and micro-strain.[29] To obtain more accurate peak information, the effect of instrumental broadening on the peak broadening was investigated by a silicon reference sample with line position and line shape standard for powder diffraction (NIST 640d). Fig. 8 distinctly shows that anatase phases of the shock-consolidated anatase TiO_2 and its starting powder contain peak broadening contribution from the silicon reference sample. The contributions from instrumental broadening, crystallite size and micro-strain can be separated as following equations.[29]

If the X-ray diffraction peaks have a Lorentzian peak shape;

$$\beta_{obs} = \beta_{size} + \beta_{strain} + \beta_{instr} \quad (1)$$

Where β_{obs} is the experimentally observed integral breadth, β_{size} is the crystallite size integral breadth, β_{strain} is the micro-strain integral breadth and β_{instr} is the instrument integral breadth. For the crystallite size and micro-strain contributions on the peak broadening, the following equation can be used.

$$(\beta_{obs} - \beta_{instr}) \cos\theta = \left(\frac{\lambda}{D}\right) + 4\varepsilon \sin\theta \quad (2)$$

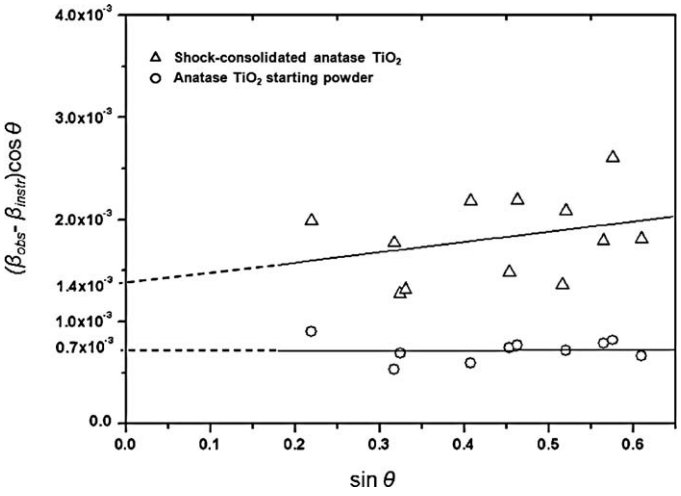

Fig. 9. Williamson–Hall plots for the shock-consolidated anatase TiO_2 and anatase TiO_2 starting powder.

where λ is the wavelength, D is the volume weighted crystallite size and ε is the weighted average strain.

If the X-ray diffraction peaks have a Gaussian peak shape, the contributions on the peak broadening can be separated as following equation:

$$\beta_{\text{obs}}^2 = \beta_{\text{size}}^2 + \beta_{\text{strain}}^2 + \beta_{\text{instr}}^2 \quad (3)$$

And for the crystallite size and micro-strain contributions;

$$(\beta_{\text{obs}}^2 - \beta_{\text{instr}}^2)\cos^2\theta = \left(\frac{\lambda}{D}\right)^2 + 4\varepsilon^2 \sin^2\theta \quad (4)$$

Since the peak (1 0 1) profiles of shock-consolidated anatase TiO_2 and its starting powder were Lorentzian peak shape, we used Eqs. (1) and (2) for the W–H plot analysis. Fig. 9 shows the W–H plots of the shock-consolidated anatase TiO_2 and its starting powder. The W–H plot slope indicates the micro-strain of a material while the intercept is a function of the crystallite size. It clearly shows the decreased crystallite size after shock-loading. The decreased crystallite size was about 110 nm on the intercept of horizontal axis. The shock-consolidated anatase TiO_2 exhibited a gentle slope due to the surface bonding between powder particles and micro-deformed strain was about $\varepsilon = 0.01$.

3.3. Photocatalytic properties

Fig. 10 shows the reflectance intensity obtained from the photocatalytic activities of shock-consolidated anatase TiO_2 using methylene blue solution. It was confirmed that a light absorption occurs at the wavelength of 500–800 nm and the reflectance intensity using the methylene blue solution after dyeing is decreased in comparison with the initial state (before dyeing). As shown in Fig. 10(a), the reflectance intensity at the wavelength of 500–800 nm was increased with increasing irradiation time after the UV-LED irradiation due to the photocatalytic effect of anatase TiO_2 compact. In particular, the photocatalytic activities were sharply increased within 5 min and gradually increased up to 10 min. Fig. 10(b) shows the photocatalytic activities of

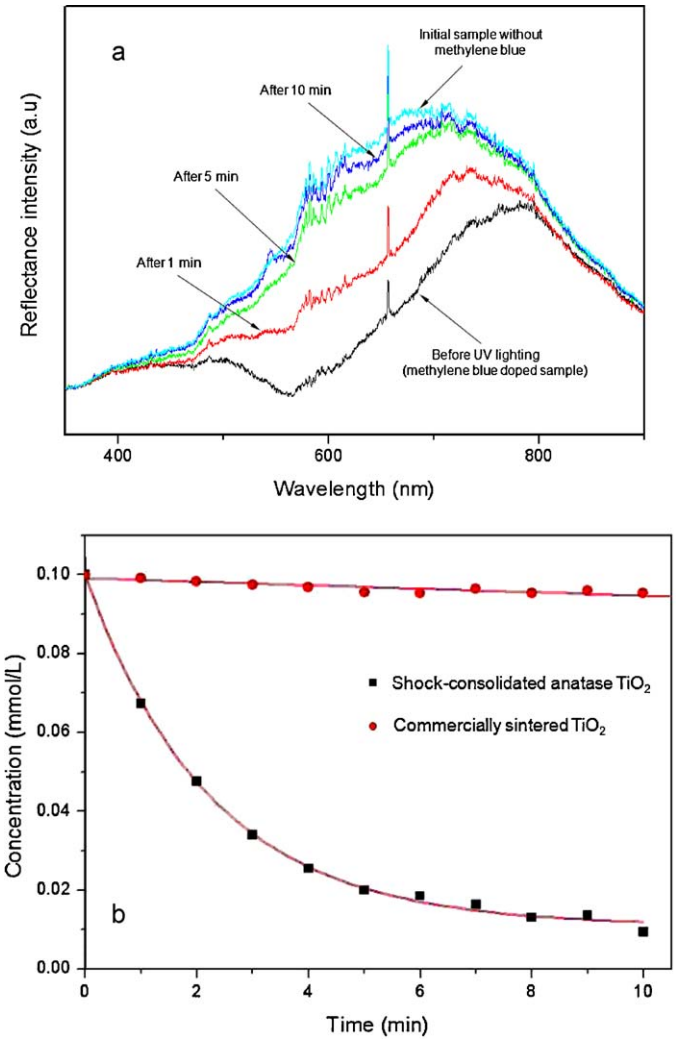

Fig. 10. (a) UV–Vis reflectance intensity obtained from the photocatalytic activity of the shock-consolidated anatase TiO_2 using methylene blue solution and (b) concentration of methylene blue as a function of the irradiation time for the shock-consolidated anatase TiO_2 and commercially sintered TiO_2.

anatase TiO_2 compact compared to that of a commercial sintered TiO_2. These results were evaluated by the decomposition of methylene blue solution at the absorption wavelength, 664.5 nm. Consequently, it was confirmed that the very fast dilution rate of 90% proceed within 10 min in the case of anatase TiO_2 compact, whereas the commercial sintered TiO_2 is very slowly diluted.

4. Conclusions

In the present work, we have successfully obtained the anatase-structured bulk TiO_2 with high purity phases and relative density of 96%, and crack-free formation at most of the areas. The microstructural, crystalline structural and photocatalytic properties were investigated. We have confirmed that the explosive compaction using an underwater shockwave induces a strong surface bonding between powder particles without a phase transformation and grain growth as well as a spalling in the anatase TiO_2 compact. In X-ray diffraction analysis, broadened peaks due to lattice defects and decreased crystallite size

were also observed in the anatase TiO_2 compact. The decreased crystallite size was about 110 nm on the intercept of horizontal axis and micro-deformed strain was about $\varepsilon = 0.01$. We have also confirmed that excellent photocatalytic activities of anatase TiO_2 compact compared to the commercial sintered TiO_2. Lastly, the authors suggest that the use of high temperature residual heat of Cu compacts generated during and after shock-loading is effective to minimize the cracking problem.

Acknowledgments

This work was supported in part by the Research Funds of Innovative Collaboration Organization of Kumamoto University in Japan.

References

1. Fujishima A, Rao TN, Tryk DA. Titanium dioxide photocatalysis. *J Photobiol C: Photochem Rev* 2000;**1**:1–21.
2. Deb SK. Dye-sensitized TiO_2 thin-film solar cell research at the National Renewable Energy Laboratory (NREL). *Sol Energy Mater Sol Cell* 2005;**88**:1–10.
3. Tang H, Prasad K, Sanjinés R, Lévy F. TiO_2 anatase thin films as gas sensors. *Sensor Actuator B* 1995;**26**:71–5.
4. Koparde VN, Cummings PT. Phase transformations during sintering of titania nanoparticles. *ACS Nano* 2008;**2**:1620–4.
5. Ahonen PP, Joutsensaari J, Richard O, Tapper U, Brown DP, Jokiniemi JK, et al. Mobility size development and the crystallization path during aerosol decomposition synthesis of TiO_2 particles. *J Aerosol Sci* 2001;**32**:615–30.
6. Hahn H, Loga J, Averback RS. Sintering characteristics of nanocrystalline TiO_2. *J Mater Res* 1990;**5**:609–14.
7. Li J, Ye Y, Shen L, Chen J, Zhou H. Densification and grain growth during pressureless sintering of TiO_2 nanoceramics. *Mater Sci Eng A* 2005;**390**:265–70.
8. Angerer P, Yu LG, Khor KA, Krumpel G. Spark-plasma-sintering (SPS) of nanostructured and submicron titanium oxide powders. *Mater Sci Eng A* 2004;**381**:16–9.
9. Lee YI, Lee JH, Hong SH, Kim dY. Preparation of nanostructured TiO_2 ceramics by spark plasma sintering. *Mater Res Bull* 2003;**38**:925–30.
10. Masahashi N. Fabrication of bulk anatase TiO_2 by the spark plasma sintering method. *Mater Sci Eng A* 2007;**452**:721–6.
11. Mazaheri M, Zahedi AM, Haghighatzadeh M, Sadrnezhaad SK. Sintering of titania nanoceramic: densification and grain growth. *Ceram Int* 2009;**35**:685–91.
12. Liao SC, Chen YJ, Mayo WE, Kear BH. Transformation-assisted consolidation of bulk nanocrystalline TiO_2. *Nanostruct Mater* 1999;**11**:553–7.
13. LaRocca EW, Pearson J. Explosive press for use in impulsive loading studies. *Rev Sci Instrum* 1958;**29**:848–51.
14. Vogler TJ, Lee MY, Grady DE. Static and dynamic compaction of ceramic powders. *Int J Sol Struct* 2007;**44**:636–58.
15. Shang SS, Meyers MA. Dynamic consolidation/hot isostatic pressing of SiC. *J Mater Sci* 1996;**31**:252–61.
16. Jordan JL, Sekine T, Kobayashi T, Li X, Thadhani NN, El-Raghy T, et al. High pressure behavior of titanium-silicon carbide (Ti_3SiC_2). *J Appl Phys* 2003;**93**:9639–43.
17. Sawaoka AB, Takamatsu M, Akashi T. Shock compression synthesis of diamond. *Adv Mater* 1994;**6**:346–54.
18. Jin ZQ, Chen KH, Li J, Zeng H, Cheng SF, Liu JP, et al. Shock compression response of magnetic nanocomposite powders. *Acta Mater* 2004;**52**:2147–54.
19. Kim Y, Ueda T, Hokamoto K, Itoh S. Electric and microstructural characteristics of bulk ZnO fabricated by underwater shock compaction. *Ceram Int* 2009;**35**:3247–52.
20. Raghukandan K, Hokamoto K, Lee JS, Chiba A, Pai BC. An investigation on underwater shock consolidated carbon fiber reinforced Al composites. *J Mater Process Technol* 2003;**134**:329–37.
21. Chiba A, Fujita M, Nishida M, Imamura K, Tomoshige R. Underwater-shock consolidation of difficult-to-consolidate powders. In: Meyers MA, Murr LE, Staudhammer KP, editors. *Shock-wave and high-strain-rate phenomena in materials*. New York: Marcel Decker; 1992. p. 415–24.
22. Shang SS, Hokamoto K, Meyers MA. Hot dynamic consolidation of hard ceramics. *J Mater Sci* 1992;**27**:5470–6.
23. Hokamoto K, Tanaka S, Fujita M, Itoh S, Meyers MA, Chen HC. High temperature shock consolidation of hard ceramic powders. *Physica B* 1997;**239**:1–5.
24. Hokamoto K, Tanaka S, Fujita M. Optimization of the experimental conditions for high-temperature shock consolidation. *Int J Impact Eng* 2000;**24**:631–40.
25. Meyers MA. *Dynamic behavior of materials*. John Wiley & Sons Inc.; 1994. pp. 523–540.
26. Meyers MA, Benson DJ, Olevsky Ea. Shock consolidation: microstructurally-based analysis and computational modeling. *Acta Mater* 1999;**47**:2089–108.
27. Bégin-Colin S, Girot T, Le Caër G, Mocellin A. Kinetics and mechanisms of phase transformations induced by ball-milling in anatase TiO_2. *J Solid State Chem* 2000;**149**:41–8.
28. Kim Y, Wada H, Lee Y, Itoh S. Magnetization, magnetic transition and magnetic entropy changes of bulk $MnAs_{1-x}Sb_x$ fabricated by underwater shock compaction. *Mater Sci Eng B* 2010;**167**:114–8.
29. Karen P, Woodward PM. Liquid-mix disorder in crystalline solid: $ScMnO_3$. *J Solid State Chem* 1998;**141**:78–88.